Mechanical characterization of lithium-ion batteries with different chemistries and formats

Journal of Energy Storage 84 (2024) 110899

Contents lists available at ScienceDirect

Journal of Energy Storage

journal homepage: www.elsevier.com/locate/est

Research papers

Mechanical characterization of lithium-ion batteries with different chemistries and formats

Davide Clerici *, Salvatore Martelli, Francesco Mocera, Aurelio Somà

Department of Mechanical and Aerospace Engineering, Politecnico di Torino, Corso duca degli Abruzzi, 24, Torino, 10129, Piemonte, Italy

ARTICLE INFO

Keywords:
Lithium-ion batteries
Experimental mechanics
Mechanical characterization
LIB thickness change
Mechanical in-operando measurement

ABSTRACT

Lithium-ion batteries undergo structural deformation during operation because of the electrochemical-induced strain caused by the insertion of lithium ions inside the active material of the electrodes.

In this work, the mechanical characteristic, i.e. thickness change, of batteries with different chemistries (lithium iron phosphate and lithium cobalt oxide) and formats (prismatic and pouch) is measured in-operando and with different current rates. A dedicated test bench is built to carry out the measurements with contactless triangulation optical sensors, sensing the displacement of the battery surfaces.

The results are critically discussed, justifying the trajectory of the thickness change observed experimentally with the mechanical properties of the electrode's active materials. Furthermore, the results obtained with the batteries of different chemistries are compared, discussing the reasons underlying these differences. Statistical considerations on the results, such as repeatability errors and cell-to-cell differences, are provided as well.

The mechanical characteristic appears as a three-stage linear curve, with two deflection points between the linear sections, and proportional to the state of charge of the battery. In fact, the mechanical characteristic tells the amount of lithium ions stored in each electrode, which together with the stoichiometric range defining the electrodes balancing, is closely related to the state of charge. Then, these measurements reveal an interesting tool for evaluating the state of charge.

The two deflection points of the mechanical characteristic are linked to graphite stage changes. Then, these measurements carry the same information about battery degradation as the peaks in differential voltage analysis. The advantage is that the deflection points remain visible at any current rate, but the peaks in the differential voltage analysis vanish at high current rates. Then, these preliminary studies of the mechanical characteristic evidence it can become a promising alternative tool for evaluating the state of health as well.

1. Introduction

The reduction of greenhouse gas emissions is the key challenge of this and the next decades to control global warming and environmental pollution. To date, 25% of greenhouse gas emissions come from transportation in the EU according to Eurostat report [1], 29% in the US according to the United State environmental Protection Agency (EPA) [2] and 15% in the world [3]. This scenario paved the way for the fast growth of zero-emission vehicles.

Nowadays, lithium-ion battery (LIB) is the leading technology able to meet the requirements of vehicles in terms of power and energy densities, causing an abrupt increase in LIB demand. Besides the good energy and power performance, LIBs have three significant drawbacks: Safety, limited life, and difficulty in estimating the internal parameters, such as state of charge (SOC), state of health (SOH), and remaining useful life (RUL).

The life of LIBs is in the order of 1000 cycles as a rule of thumb, and it strongly depends on current and temperature. Then, its life cycle is possibly shorter than the vehicle's life [4,5]. The limited battery life raises the issue about the management of LIBs at end of life (EOL) (second life, recycling, disposal), as well as the issue about understanding how far the LIB is from EOL and how to recognize the EOL. Indeed, a sensor able to measure the SOH or the RUL does not exist, and these parameters must be estimated from what can be measured: voltage, temperature, and current, traditionally. However, the SOH or RUL estimation from voltage, temperature and current is extremely challenging because of the complex multi-physics nature of LIBs. Indeed, physics-based models can be accurate, but the high number of physical parameters difficult to estimate, and the model complexity hinder their application for on-board estimation purposes in battery management systems (BMS). These drawbacks may be overcome by neural-network-based algorithms, which, on the other hand, rely on

* Corresponding author.
E-mail address: davide.clerici@polito.it (D. Clerici).

https://doi.org/10.1016/j.est.2024.110899
Received 26 July 2023; Received in revised form 20 January 2024; Accepted 8 February 2024
Available online 15 February 2024

huge amounts of data, specific of a certain battery model, and suffer poor interpretability and generalization. Furthermore, considering an average length of several months for accelerated cyclic aging tests up to years for calendar aging tests in a laboratory, the data collection becomes extremely time-consuming.

Besides SOH and RUL, SOC is another key parameter necessary to be known for the correct management of the LIB during usage. Again, a sensor able to estimate SOC does not exist, and it must be estimated from voltage, temperature and current measurements, facing all the difficulties explained before for SOH and RUL estimation.

Mechanics has a significant role in LIBs, both as a damaging cause, due to the rise of mechanical stress in the electrode microstructure during operation [6–11], and consequent crack propagation [12–16], both as a way to estimate battery internal parameters, measuring its mechanical deformation.

In the last years, especially since 2020, mechanical measurements have attracted increasing attention because of their ability to carry important information about the SOH and SOC of the LIB. In this regard, Popp et al. [17] proposed an interesting review of the mechanical methods for state determination of LIB. In literature, mechanical measurements have been carried out with optical displacement sensors [18–20], strain gauges [21,21,22], internal pressure sensors [23], pressure sensors [24–30], dial indicator [31–37], load cells [38–42], fiber optics [43–46] and eddy current sensors [47–49].

LIBs store and withdraw electrical energy thanks to the electrochemical reactions involving lithium ions and the active material of anode and cathode. During charge, lithium ions are deintercalated from the positive electrode, travel through the separator and intercalate into the negative electrode. The greater the state of charge of the battery, the greater the amount of lithium stored in the negative electrode with respect to the positive electrode. Vice-versa during discharge. When lithium ions intercalate into the lattice structure of the electrode they cause its structural deformation. At the macroscopic level, this results in the battery "breath": LIBs swell during charge and the swelling is reversibly recovered during discharge, because of the relative mechanical properties of the anode and cathode. Several works also modeled LIB deformation from the atomic scale to the battery scale with multiscale approach [24,32,35,50,51]. Then, the swelling of the battery is proportional to the number of lithium ions stored in the anode with respect to the cathode, which together with the stoichiometric range defining the electrodes balancing, is closely related to the SOC. As a consequence, this characteristic makes the mechanical deformation a promising tool to estimate SOC, and it may overcome some of the limits of voltage: (a) Voltage plateaus, where small changes in voltage correspond to large changes in SOC; (b) Polarization, making the voltage strongly dependent on the applied current.

Recently, several authors developed a SOC estimator based on solely LIB swelling characteristics, or together with electrical parameters and temperature. Mainly, two approaches were followed: model-based approach with the Kalman filter estimator [52,53], and neural network models [54]. Jiang et al. [55] estimated SOC based on battery expansion with deep neural network, obtaining an RMSE of about 2%. Interestingly, Ee et al. [43] compared the SOC estimation with deep neural networks based on electrical and non-electrical (strain and temperature) parameters. In the case of non-electrical parameters, they obtained a 1% RMSE, lower than the estimation based on solely electrical parameters. Peng et al. [45] estimated SOC both with Unscented Kalman filtering and with a two-hidden layer artificial neural network. The unscented Kalman filter was solely based on strain, which was modeled with the multiple linear regression method, getting a polynomial that correlates strain with current and SOC. A good accuracy was got in the SOC estimation both with constant current cycles and dynamic cycles with this method. On the other hand, the neural network method took as input voltage, current, temperature, and strain. The results showed that the accuracy was slightly better than the unscented Kalman filter model, and the inclusion of strain and temperature had a negligible influence on the error reduction.

About the model-based approach, Mohan et al. [38] related SOC to bulk force, temperature and current, and provided a mathematical explanation supporting the benefits of LIB swelling in SOC estimation, particularly in the low SOC range (30%–50%). Figueroa et al. [40] compared the SOC estimated with the Kalman filter based on voltage and swelling or voltage alone, showing that the inclusion of voltage improved the estimation, especially in those cases, such as lithium iron phosphate (LFP), where voltage is flat with respect to SOC. Dai et al. [42] found a mathematical correlation between stress exerted by pouch battery surface over a constraint and SOC, which is at the basis of their estimation algorithm. Finally, Rente et al. [46] estimated SOC with a dynamic time-warping technique, based on strain and temperature measurements.

Irreversible swelling occurs during aging, meaning that some extent of the swelling during charge is not recovered during discharge, and the battery constantly increases in volume with repeated charges and discharges cycles [22,25,26,45,56], probably because of the growth of the solid electrolyte interphase (SEI) layer [30]. This behavior allows relating the SOH with the amount of irreversible swelling, improves the estimation correcting mismatched initial values and eliminating cumulative errors [45].

Together with irreversible swelling, the reduction of reversible swelling is usually observed with aging, because of the decrease of capacity and cyclable lithium ultimately [34,56], but this trend is not in agreement with the works of other authors, who observed an increase of reversible swelling with aging [22].

Irreversible swelling is not the only way to keep track of SOH. Cannarella et al. [26] was the first to observe the connection between the graphite phase transitions and the LIB swelling, relating the peaks in differential voltage analysis (DVA) with the peaks in the second derivative of the LIB swelling. This method can be used, exactly as DVA, to quantify SOH [26,31,33,39]. The advantage with respect to DVA is the improvement of the SOH estimation at higher SOC and with higher current [31,39].

From this literature review, mechanical measurements appear well suited for SOC and SOH estimation, resulting in several patents [57–63]. These considerations motivate an in-depth and structured study of the mechanical characteristic of different LIBs, both in terms of chemistry and formats.

The objective of this work is to carry out a rigorous experimental study on the mechanical behavior of lithium-ion batteries with different chemistries and formats. To this end, LFP-graphite prismatic and lithium cobalt oxide (LCO)-graphite pouch LIBs are considered because of the significantly different mechanical behavior of LFP with respect of LCO. Furthermore, the aim of the work is also to highlight potential features of the mechanical characteristic of LIB in the view of state estimation based on mechanical measurements.

In the work methodology, the following aspects represent a novelty according to the authors:

- Mechanical measurements are carried out with contactless sensors, while usually load cells or optical fibers are used for such measurements. Optical fibers give strain measurements which are difficult to link to the volume change of the battery, while load cells exert a force on the battery sample, potentially affecting its mechanical behavior.
- Statistical study of the results. The tests are repeated five times on the same sample, and three samples per chemistry are considered. This allows studying the repeatability of the measurement and cell to cell variations. These are valuable information in the view of adopting mechanical information as an additional measurement for battery state estimation.

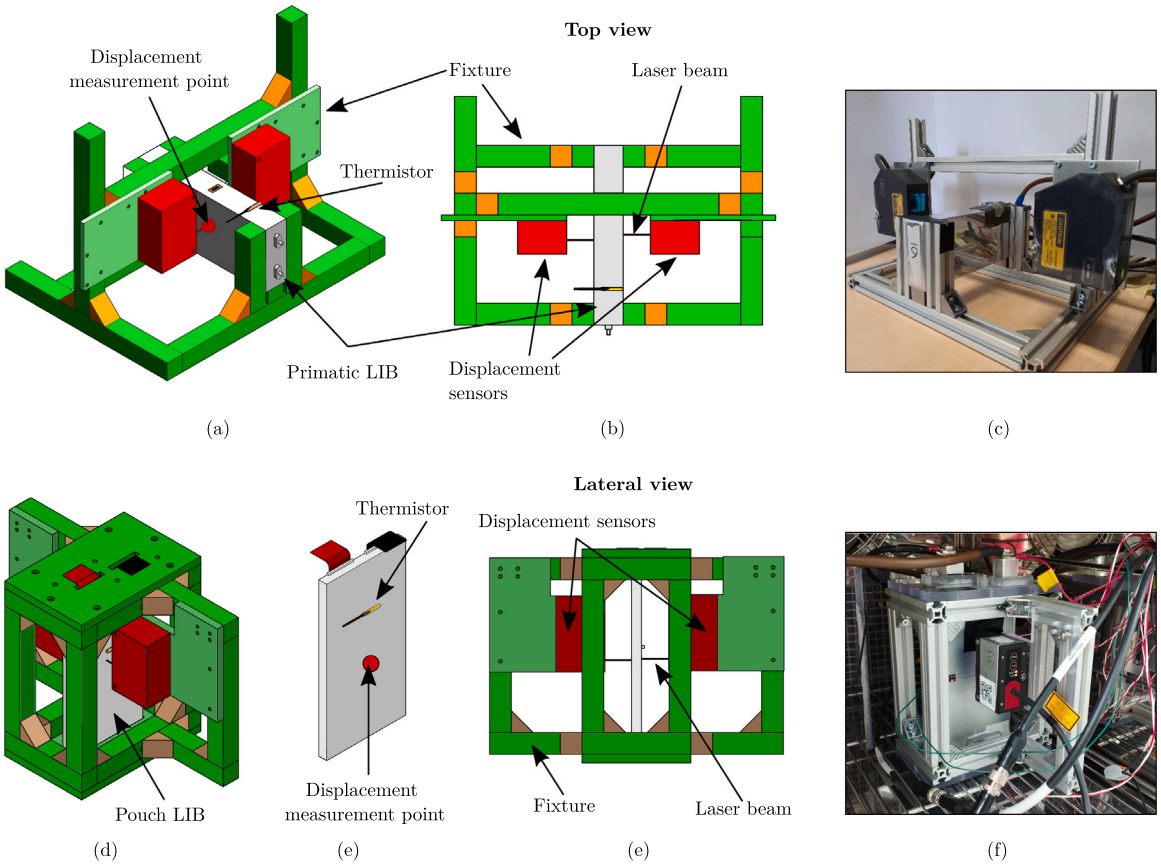

Fig. 1. Description of the measurement set-up designed by the authors for the prismatic LFP (**a**)-(**c**) and the pouch LCO (**d**)-(**f**) batteries.

- Comparison of mechanical measurements on batteries with different chemistries. Indeed, LFP has the higher lithiation-induced swelling among cathodes, while LCO shrinks during lithiation. This comparison highlights how the mechanical behavior of the negative electrode dominates the mechanical deformation of the battery. It is highlighted that graphite is used as a negative electrode in the battery samples tested in this work and in most of commercial batteries, making the results observed in this work similar to what can be expected from most of commercial batteries.
- Finally, it is highlighted how the influence of the format (pouch or prismatic) affects the mechanical measurements.

2. Methods

Prismatic LFP and pouch LCO battery samples were mechanically characterized during charge and discharge cycles at different current rates. The energetic size of the two types of batteries is similar, and the summary of the batteries' properties is reported in Table 1.

The test bench used for the in-operando mechanical characterization consists of a power supply "QPX600DP" by Aim-TTi and an electronic load "EL 9080-400" by Elektro-Automatik. The batteries are sensorized with a thermistor, and a couple of optical displacement sensors "optoNCDT 1900-10LL" by MicroEpsilon for thickness change sensing. The benchmark is controlled in real-time by the National Instruments controller "NI PXIe-8840". The ambient temperature is controlled with a climatic chamber by MSL.

The distance sensors have a linearity error of ±2 μm, which is about 0.5% of the maximum displacement measured by each sensor during the tests. The optical sensors are mounted on a dedicated structure designed by the authors which ensures the perpendicularity between the laser beam and the LIB surfaces and keeps fixed the LIB during the acquisition process, as shown in Fig. 1a-c (prismatic LIB) and Fig. 1d-f (pouch LIB). Thickness change measurements were carried out in the central point of the larger surfaces of the LIBs, as shown in Fig. 1a,e.

The mechanical measurements were conducted during operation at different current rates: discharge was carried out at C/20, C/5, C/2, 1C, 2C, 3C (and 5C just on LCO), charge at C/20, C/5, and C/2, according to manufacturer limits. Discharge is carried out with continuous current (CC) until cut-off voltage (2,5 V for LFP and 3 V for LCO), charge begins with CC, when cut-over voltage (3,65 V for LFP and 4,2 V for LCO) is reached, a constant voltage is kept until the current drops below C/20.

The tests are repeated five times on the same LIB for each current rate, then the same procedure is carried out on three different samples of LFP and LCO batteries.

Table 1
LIBs samples properties. The current rate is expressed in C-rate, where 1C is the current needed to completely discharge the battery in one hour.

	LFP	LCO
Manufacturer	Topband	Melasta
Anode	Graphite	Graphite
Cathode	LFP	LCO
Type	Prismatic	Pouch
Length	180 mm	182,5 mm
Width	70 mm	94,5 mm
Thickness	27 mm	9,2 mm
Capacity	25 Ah	22 Ah
Operating voltage	2,5 V–3.65 V	3 V–4,2 V
Max operating current charge	C/2	C/2
Max operating current discharge	3C	5C
Thermal expansion coefficient	$2,5\,10^{-4}$ °C^{-1}	$2,0\,10^{-4}$ °C^{-1}

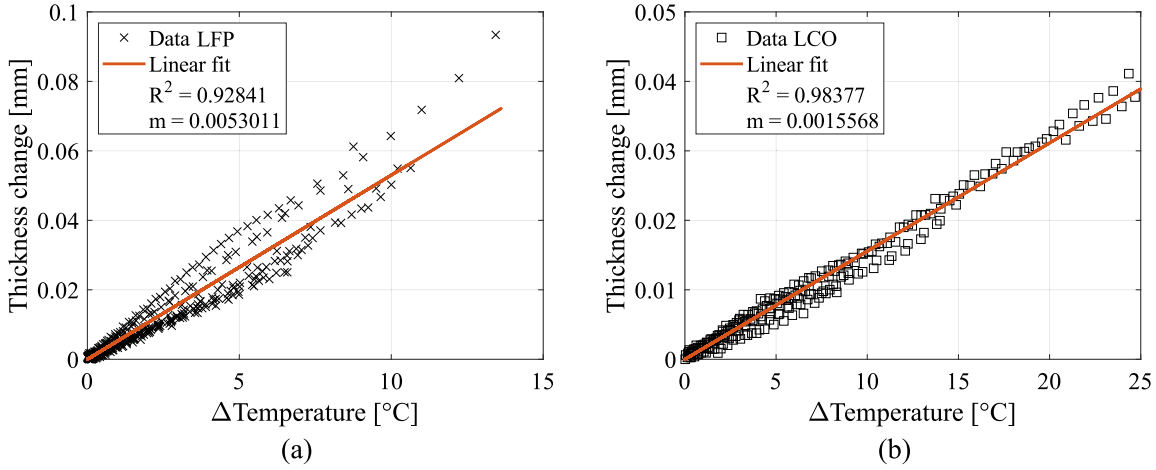

Fig. 2. Identification of thermal expansion coefficient. Thickness change as a function of temperature difference during cool-downs after operation on (**a**) LFP and (**b**) LCO battery samples. The parameter m refers to the slope of the linear fit ($\frac{\Delta t_{LIB}}{\Delta T}$).

LIBs temperature rises during operation, because of joule heating, irreversible (proportional to overpotential), and reversible processes. As a consequence, both electrochemical processes (lithium insertion and extraction) and temperature changes affect the mechanical characteristic of the batteries. For this reason, LIBs temperature was recorded on the external surfaces during the tests, to identify the thermal contribution to the thickness change measurements.

Thermal deformation coefficient was measured experimentally monitoring how the LIBs thickness changed during cool down after discharge when no current was applied. To explore a possible SOC dependency, LIB samples were discharged until different SOC levels and then let cool. As shown in Fig. 2, a linear relationship exists between thickness change and temperature during cool down. No dependence of the thermal expansion coefficient on SOC was observed, in agreement with previous works [64]. This method is more effective than changing the temperature inside the climatic chamber because the fixture where the optical sensors are mounted keeps the same temperature, avoiding its thermal deformation which would affect the displacement measurement.

Then, the thermal expansion coefficient (α) is calculated in Eq. (1) knowing the slope ($m = \frac{\Delta t_{LIB}}{\Delta T}$) of the linear fit of data in Fig. 2.

$$\alpha = \frac{1}{t_{nom}} \frac{\Delta t_{LIB}}{\Delta T} \tag{1}$$

Where t_{nom} is the nominal thickness of the battery sample.

The temperature was kept at 20 °C inside the climatic chamber during the tests.

3. Results and discussion

3.1. Voltage

Voltage measurements of LFP and LCO batteries are reported in Fig. 3a, c and Fig. 3b, d, respectively.

Stage transitions of graphite can be identified by the sudden drop of voltage measurements at SOC 30% and 65% in LFP battery samples and at SOC 25% and 60% in LFP battery samples. It will be shown that these drops match the deflection points of the mechanical characteristic curve. Furthermore, these drops become unobservable at progressively higher current rates.

The rate capability of LCO batteries is quite poor, especially in comparison to LFP batteries, as the capacity extracted during discharge drastically falls at higher current rates, as well as the voltage provided by the battery.

3.2. Temperature

Temperature measurements of LFP and LCO batteries are reported in Fig. 4a, c and Fig. 4b, d, respectively. From the temperature point of view, LCO batteries result significantly more exothermic with respect to LFP, especially at high current rates.

The ripple visible in the low rate charge and discharge curves of the LCO battery is reasonably caused by the reversible heat, namely the heat caused by entropy change and the temperature dependence of the open circuit voltage. Being reversible, it can be released or stored in the battery according to its voltage, and then temperature increases and decreases accordingly. The reversible heat does not depend on current, then its influence vanishes at high current rates, where the irreversible and joule heats prevail. The trend of the entropy (dU/dT) measured on LCO electrodes by Thomas and Newman [65] supports this reasoning: It is clear that the steep ripple at $y = 0.6$ in Li_yCoO_2 in their entropy measurements is in agreement with the ripple at SOC 80% in the measurements in Figs. 4b, d.

3.3. Thickness change

The thickness change curves of LFP and LCO batteries during discharge and charge are reported in Fig. 5a, c and Fig. 5b, d, respectively.

Both LFP and LCO batteries shrink during discharge and swell during charge. This behavior is due to the mechanical properties of the electrodes: graphite, which is the negative electrode material in both batteries, has greater partial molar volume than active materials used in the positive electrodes. Partial molar volume is the proportionality coefficient between electrochemical-induced strain and solute (lithium ions) concentration, according to Eq. (2) [7].

$$\varepsilon_e = \frac{1}{3} \int_{c_{sf}}^{c} \Omega dc \tag{2}$$

Where ε_e is the electrochemical-induced strain, c_{sf} is the reference concentration at zero strain, Ω is partial molar volume and c is the lithium-ions concentration.

Then, for example during charge, graphite expansion is greater than the shrinkage of the positive electrode, causing the overall LIBs swelling. Vice-versa, LIBs shrink during discharge. Furthermore, LCO has a negative partial molar volume, meaning that it shrinks when lithiated.

LCO batteries show a greater absolute thickness change, nearly $0,3$ mm with respect to $0,2$ mm of LFP batteries. In general, the amount of volume deformation depends on the quantity of active material (proportional to the battery capacity), the volume deformation of the

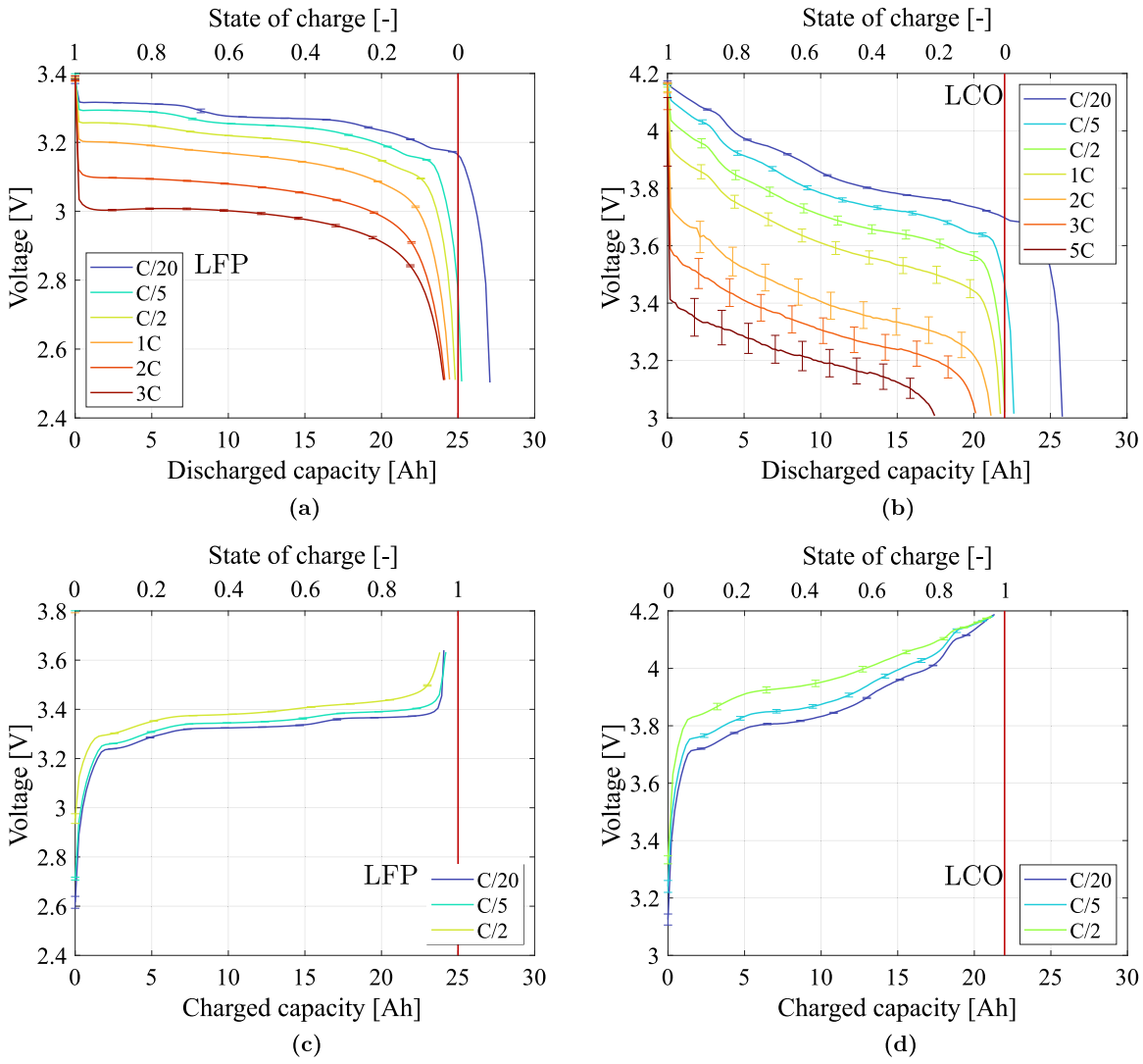

Fig. 3. Voltage response at different current rates of LFP battery samples during discharge (**a**) and charge (**c**), and LCO battery samples during discharge (**b**) and charge (**d**). Solid lines refer to the mean value between all the measurements carried out on all the samples and the error bars to the total standard deviation. The vertical red line indicates the nominal capacity.

active materials, and possibly the LIB format. Capacity is similar, even if LFP battery samples have a slightly greater capacity. Anode active material is the same, but LFP has about $6,53\%$ deformation when fully lithiated [19,66], with respect to -2% of LCO [67]. This means that during charge, the expansion of graphite (about 10% at $Li_{0,75}C_6$ which corresponds to SOC 100% [19]) is counterbalanced by the shrinkage of the positive electrode being delithiated ($-6,53\%$) in LFP batteries.

On the other hand, in LCO batteries both the negative and positive electrode swell during charge, because of the peculiar behavior of LCO, which swells when delithiated. This is the most significant reason why LCO batteries show greater absolute volume change with respect to LFP batteries.

The format of the battery does not play a significant role in LIB deformation: The rigid case of prismatic batteries slightly hinders volume change, constraining the inside of the LIB, but the amount of thickness change prevented has been quantified lower than 10% according to a structural finite element model carried out in authors' previous work [19].

The thickness change curves of LFP and LCO batteries have a similar trajectory: a three-stage linear piecewise function, where the three linear sections are separated by two deflection points, at SOC about 30% and 60%. This trend is caused by the graphite deformation, which is used as an anode in both LFP and LCO batteries. Graphite has a non-constant partial molar volume, resulting in a non-linear deformation with respect to the moles of lithium ions inserted (refer to Eq. (2)). This behavior is due to stages formation in the crystalline structure of graphite with different atomic arrangements and then geometric dimensions [68].

In particular, stage II, which corresponds to $Li_{0,5}C_6$ and it has the major content when the battery SOC is in the range 30%–60%, has a significantly lower partial molar volume, about $1\ cm^3/mol$ (some differences exist between charge and discharge) with respect to the other stages, about $5-7\ cm^3/mol$ [19]. This makes the overall battery deformation trend to decrease, or even invert (passing from swelling to shrinkage or vice-versa), in the SOC range 30%–60%. In particular, the thickness change of LFP batteries inverts its trend in the SOC range 30%–60% both in charge and discharge, as observed in Fig. 5a, c. On the other hand, the thickness change trend of LCO in the SOC range 30%–60% just decreases, as observed in Fig. 5b, d.

The discerning element of the possible inversion of the thickness change trend is the value of the partial molar volume of the cathode in the battery SOC range 30%-60%: if it is greater than graphite ($1\ cm^3/mol$), the thickness change inverts its trend.

In the case of LFP batteries, LFP has a constant partial molar volume equal to $3\ cm^3/mol$, greater than the one of stage II of graphite, then

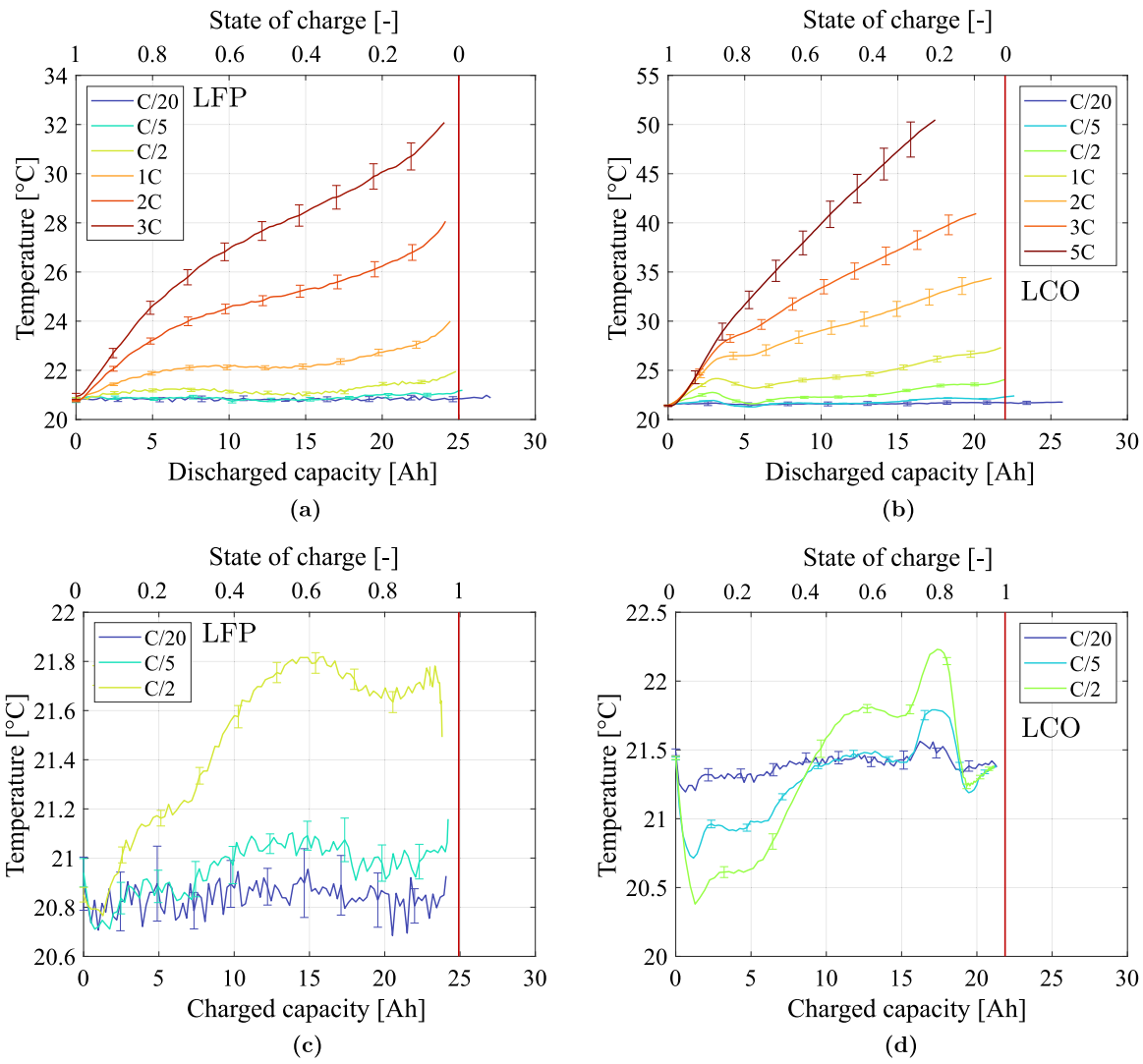

Fig. 4. Temperature response at different current rates of LFP battery samples during discharge (**a**) and charge (**c**), and LCO battery samples during discharge (**b**) and charge (**d**). Solid lines refer to the mean value between all the measurements carried out on all the samples and error bars to the standard deviation. The vertical red line indicates the nominal capacity.

the shrinkage of LFP during charge overcomes the reduced graphite expansion in the central SOC range 30%–60%, causing the battery to shrink during charge in this SOC range.

On the other hand, LCO has a negative partial molar volume, then deformation is always monotonic as the positive and negative electrodes swell (or shrink) simultaneously during charge (or discharge). Nevertheless, the swelling of the LCO batteries slows down in the SOC range 30%–60%, and the curve deflection points at the boundaries of this range remain visible. Interestingly, these deflection points occur at approximately the same SOC value, both in LCO and LFP batteries, at about SOC 30% and 60%, meaning that the lithiation window of graphite in both the battery is similar ($Li_{0,05}C_6$-$Li_{0,75}C_6$ approximately).

From these considerations, it is evident that the two deflection points in the thickness change curve identify stage transitions in graphite, even when compared to the voltage drops observed in Fig. 3. The identification of the stage transitions of graphite with respect to SOC is a strategic tool to identify battery degradation and capacity fade, and will be deepened later by discussing SOH estimation.

Thickness change curves at different current rates are similar during charge (Figs. 5c-d), because the electrochemical-induced deformation of the active materials does not depend on the lithiation rate, and because the temperature change is not significant, then the volume deformation associated to thermal phenomena. On the contrary, thickness change curves change trajectories with different current rates during discharge (Figs. 5a-b). This is particularly evident at the higher current rates because temperature change and the associated thermal deformation become significant. Anyway, in LCO batteries the current rate dependence looks less apparent because the partial molar volume of LCO does not stand out the current rate dependency of partial molar volume of graphite, and because of the lower thermal contribution to thickness change of LCO batteries.

The thermal contribution to thickness change is quantified in Eq. (3) and reported as dashed lines in Fig. 6a-b.

$$\Delta t_{thermal} = \alpha t_{nom} \Delta T \tag{3}$$

Where $\Delta t_{thermal}$ is the thermal contribution to thickness change, α and t_{nom} are the thermal expansion coefficient and the nominal thickness of the batteries, reported in Table 1 and ΔT is the temperature change during the test, reported in Fig. 4.

Then, the electrochemical contribution to thickness change is calculated by subtracting the thermal contribution from thickness change measurements (dotted lines in Figs. 6a–b), and is reported in Fig. 6 with solid lines together with standard deviation (Figs. 6c–d).

It is observed that in the LCO batteries, the low nominal thickness of the battery (9 mm with respect to 27 mm of the LFP) makes the thermal

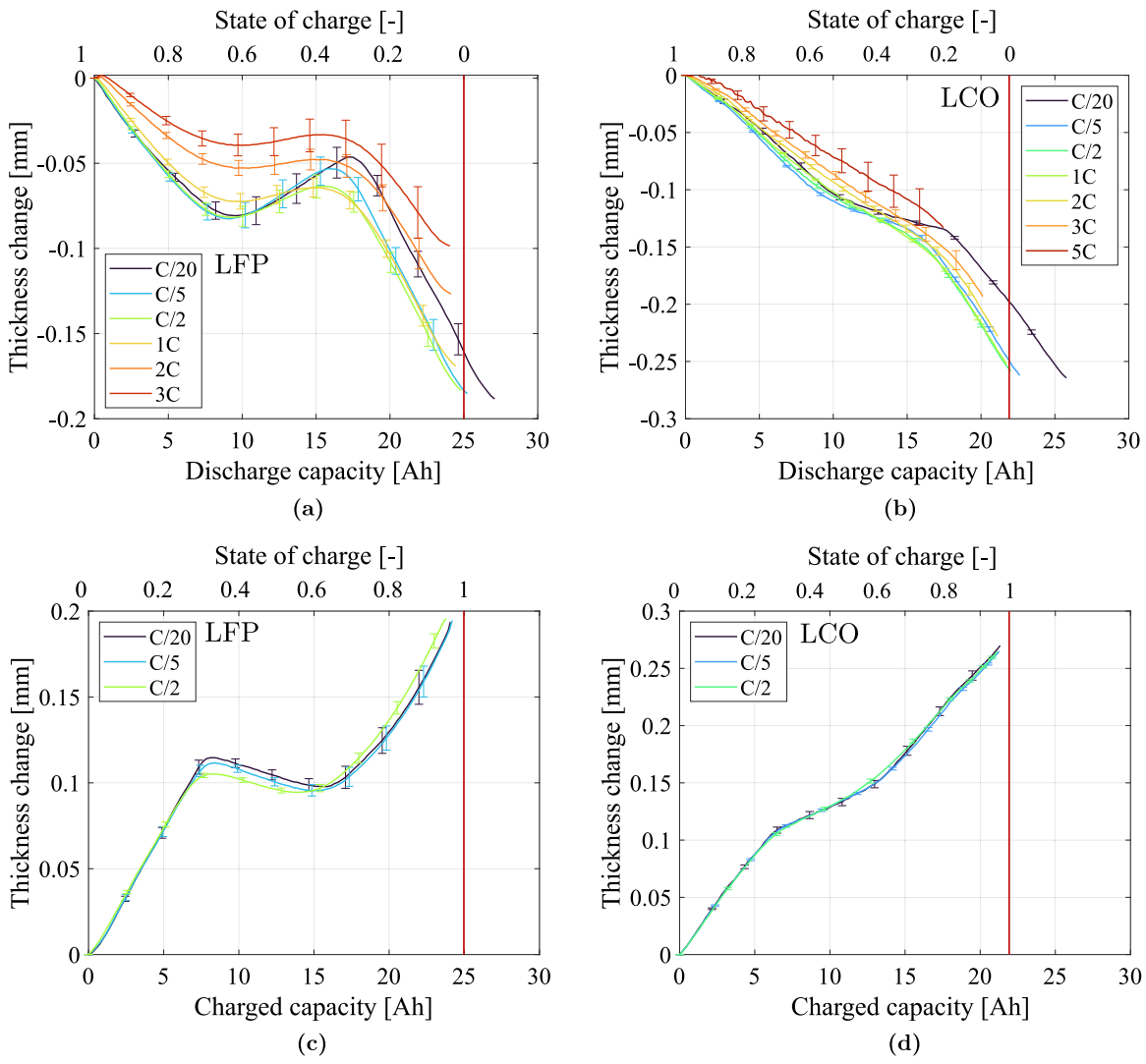

Fig. 5. Thickness change response at different current rates of LFP battery samples during discharge (**a**) and charge (**c**), and LCO battery samples during discharge (**b**) and charge (**d**). Solid lines refer to the mean value between all the measurements carried out on all the samples and the error bars to the total standard deviation. The vertical red line indicates the nominal capacity.

induced thickness change less pronounced, even if the temperature are higher (40 °C for the LCO vs 28 °C for the LFP at 3C).

Temperature is not the only responsible for the different trajectories followed by the thickness change curves at different discharge rates. Observing the electrochemical-induced thickness change curves in Fig. 6c–d, it is evident that the curves still follow different trajectories changing the discharge rate, both in LFP and LCO batteries. In particular, the second deflection point at SOC 30% is observed to decrease increasing the current rate.

This happens because graphite follows a different delithiation path going from stage III to stage II changing the discharge (delithiation) rate. Indeed, stage IIL (characterized by greater volume than stage II) appears at a low discharge rate and gradually disappears increasing the current (delithiation) rate, to the advantage of stage II. This behavior makes the second deflection point (at SOC 30%) to gradually decrease its volume because of the increasing content of stage II at the expense of stage IIL. Furthermore, stage IIL does not appear during graphite lithiation (charge), then the deflection point at SOC 30% has a lower volume during charge, similar to the one at a high discharge rate, and is not affected by the charge rate.

In the view of SOC and SOH estimation with mechanical measurements, just the electrochemical-induced thickness change must be considered, even if not explicitly specified in the next lines.

The thickness change of LFP and LCO batteries is proportional to battery capacity, then it is an effective way to estimate SOC. Nevertheless, some difficulties may be encountered when dealing with cathode materials with partial molar volume locally greater than graphite in the SOC range 30%–60%, such as LFP. In those cases, the LIB locally inverts its deformation trend (shrinks during charge and swells during discharge) in the SOC range 30%–60%, resulting in an overall non-monotonic thickness change trend, as explained earlier and reported in Fig. 5a, c.

As explained before, the thickness change trend of LFP is non-monotonic and the one of LCO is monotonic, because of their partial molar volume. Considering other materials, NMC has a partial molar volume slightly lower than graphite, about $0,5\ \mathrm{cm}^3/\mathrm{mol}$ at high lithiation index [69] corresponding to battery SOC 30%–60%, resulting in a monotonic thickness change curve [32,36].

The possible non-monotonic trend complicates the SOC estimation because one thickness change value corresponds up to three possible SOC values. To overcome this issue, Figueroa et al. [40] modeled the force-SOC (similar to thickness change-SOC) relation with a piecewise linear function, based on the positions of the deflection points at SOC 30% and 60%. The accuracy of this method strongly relies on the correct SOC position of the deflection points, which may shift during

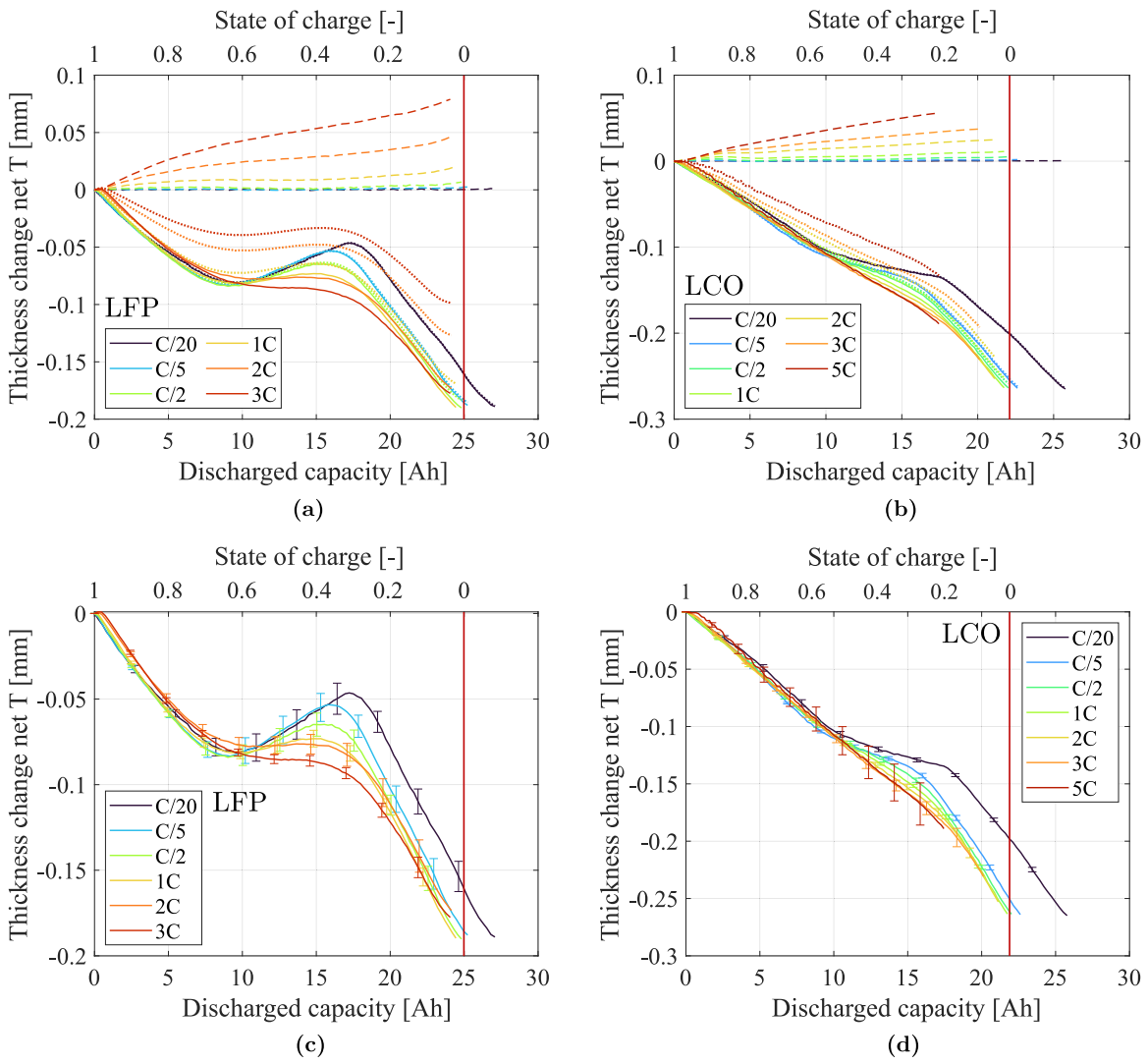

Fig. 6. Thickness change contributions at different current rates of LFP (**a**) and LCO (**b**) battery samples during discharge. Dotted lines correspond to measurements, solid lines to electrochemical contribution, and dashed lines to thermal contribution. Electrochemical contribution to thickness change and total standard deviation of LFP (**c**) and LCO (**d**) batteries during discharge. The vertical red line indicates the nominal capacity.

LIB aging. To this end, a robust SOC estimation algorithm may embed a SOH estimator as well.

In conclusion, in the case of graphitic anode, the active materials with partial molar volume lower than 1 cm^3/mol in the SOC range 30%–60% (such as NMC and LCO) will result in a monotonic battery swelling behavior, simplifying the algorithm of SOC estimation. In the other cases, a non-monotonic thickness change trend will occur.

The tests presented in this work do not consider how the mechanical characteristic of the battery change with aging, but knowing its shape, some consideration about SOH can be done as well.

SOH can be estimated from mechanical measurements leveraging two characteristics: Irreversible swelling and the shift of the deflection points. Clearly, nothing can be said about the irreversible swelling from this work.

Differential voltage analysis (DVA) is one of the most popular analyses to accurately evaluate battery degradation. It consists in analyzing how the peaks in the curve obtained as the derivative of voltage with respect to capacity shift with respect to the SOC during aging [70]. The method is accurate but can be applied just at a very low current. Indeed, as can be observed from voltage measurements in Fig. 3, the little drops in voltage disappear at high current rates. On the other hand, the mechanical characteristic does not suffer polarization as voltage, and the deflection points remain visible even at a higher current. The shift of the deflection points of the mechanical characteristic are usually traced by the second derivative of the thickness change (or any mechanical characteristic). In those cases when the inversion of the mechanical characteristic occurs in the SOC range 30%–60% (such as in LFP batteries), the shift of the deflection points may be simply followed by tracking the zero of the first derivative of the mechanical characteristic, because the deflection points are local peaks with zero derivative, as illustrated in a recent patent by authors' research group [63]. This method has two main advantages: it has an easier implementation and causes fewer errors. Indeed, finding the zero of a function is easier than finding a peak. Furthermore, the derivation of a measurement amplifies the noise, then an estimation based on a lower derivation order improves the accuracy, especially with noisy data.

In the end, from the analysis of the mechanical measurements reported in Figs. 5–6, it turns out that LIB with non-monotonic mechanical characteristic, such as LFP, may be problematic for SOC estimation, but good for SOH estimation. The other way around, LIB with monotonic mechanical characteristic, such as LCO and NMC, have easier SOC estimation algorithms but more complex SOH estimators, if based just on mechanical measurements.

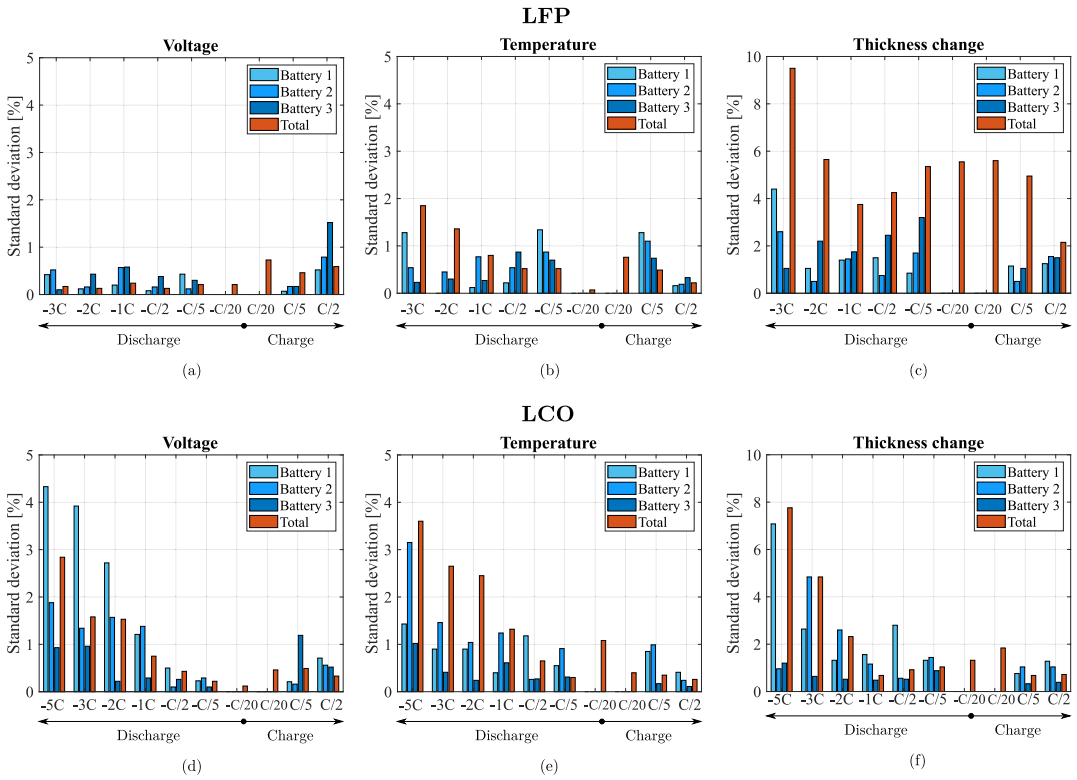

Fig. 7. Standard deviation of voltage, temperature, and thickness change measurements on LFP **(a)–(c)** and LCO **(d)–(f)** battery samples. The blue columns refer to the standard deviation among the measurements carried out on the same battery sample, and the red column labeled "total" refers to the standard deviation among all the measurements carried out on all the battery samples, highlighting the cell-to-cell differences.

3.4. Statistical considerations

Two types of measurement errors are taken into account: repeatability error and cell-to-cell differences. The first takes into account the error among repeated measurements with the same operating condition (current rates), and is calculated as the standard deviation of the measurements on a certain sample with a certain operating condition, as reported in Eq. (4)a. The latter considers the discrepancies of the measurements, carried out with the same operating conditions, among different battery samples of the same chemistry (cell-to-cell differences), and is calculated as the standard deviation of all the measurements carried out on all the battery samples for a certain operating condition, as reported in Eq. (4)b. Both the standard deviations in Eq. (4) are then normalized with respect to the mean, to get a percentage error.

$$SD_{Batt} = \sqrt{\frac{\sum_{i=1}^{N_{test}} (x_n^i - \hat{x_n})^2}{N_{test} - 1}} \tag{4a}$$

$$SD_{Total} = \sqrt{\frac{\sum_{n=1}^{N_{sample}} \sum_{i=1}^{N_{test}} (x_n^i - \hat{x_{tot}})^2}{N_{test} \cdot N_{sample} - 1}} \tag{4b}$$

Where SD_{Batt} is the repeatability error, SD_{Total} is the cell-to-cell error, N_{test} is the number of tests carried out on the same battery sample with a certain current rate, N_{sample} is the number of battery samples considered, x_n^i is the ith measurement with a certain current rate carried out on the battery sample n, $\hat{x_n}$ is the mean of the measurements with a certain current rate carried out on the battery sample n, $\hat{x_{tot}}$ is the mean of the measurements with certain current rates, carried out on all the battery samples.

Repeatability errors are reported in Fig. 7 as shaded blue columns for each battery sample, and cell to cell error is reported as a red column and labeled as "Total".

If blue columns have comparable height with respect to the red column, it means that repeatability error is dominant, and cell-to-cell error is just a consequence. If the height of the red column is substantially greater than the blue columns, it means that cell-to-cell error is dominant. These errors are calculated separately for LFP and LCO batteries.

Voltage measurements show negligible errors and excellent consistency among different LFP battery samples, as shown in Fig. 7a. For what concerns LCO batteries, an increasing error is observed increasing the current rate (Fig. 7d), mainly due to repeatable errors, as the standard deviation of the measurement on the single cells is comparable to the overall standard deviation.

Temperature shows little variation among LFP batteries (Fig. 7b), and slightly greater cell-to-cell differences in LCO batteries (Fig. 7e), especially at higher rates.

The repeatability error on the thickness change measurements on LFP and LCO batteries on the same sample is satisfactory, as the standard deviation of the measurements on each sample is lower than 2%, except for some cases at the highest current rates, according to Figs. 7c, f. For LCO batteries, cell-to-cell differences are negligible, except for high current rates. On the other hand, LFP batteries show greater cell-to-cell differences, with an overall standard deviation of about 6%. It is observed both in LFP and LCO batteries that higher current rates affect the consistency of thickness change measurements carried out on the same LIB, causing repeatability errors.

4. Conclusion

The results of the in-operando measurements of the mechanical characteristic in terms of thickness change of batteries with different chemistries (LFP and LCO) and formats (prismatic and pouch) subjected to different charge and discharge rates are shown in this work. The errors in terms of repeatability and cell-to-cell differences are generally low, about 5%, and always lower than 10%, except few cases.

The interpretation of the thickness change trajectory is provided based on the chemo-mechanical properties of the active materials of the anode and cathode and the thermal properties of the LIBs. In particular, it is observed that graphite dominates the deformation trend, overcoming the opposite deformation of the positive electrode during operation and giving the distinguishable linear three-stage shape to the mechanical characteristic of the battery, regardless of the active material of the positive electrode.

Nevertheless, the partial molar volume of the active material of the positive electrode is the discerning element from monotonic and non-monotonic trend of the mechanical characteristic. Partial molar volume is the proportionality constant between material deformation and lithium concentration. Generally, the partial molar volume of graphite (negative electrode) is greater than the positive electrode, making the battery swell during charging, and shrink during discharging. Nevertheless, the partial molar volume of graphite is not constant with lithium concentration and drastically decreases in the central SOC region (30%–60%). In this range, if the partial molar volume of the positive electrode overcomes graphite (1 cm^3/mol), such as in LFP batteries, a non-monotonic mechanical characteristic occurs.

The analysis of the features of the mechanical deformation of LIBs during operation highlights its potential application in the SOC and SOH estimation algorithms, together or as alternative to voltage. Indeed, mechanical deformation is proportional to the mean concentration of lithium ions in the electrode, thus to the state of charge. Furthermore, when compared to voltage, it is less influenced by the applied current and does not show plateaus hindering the estimation. Secondly, the turning points of the mechanical characteristic are linked to graphite stage transitions and can be used to estimate battery degradation [63] as in DVA, with the advantages that such traces do not vanishes increasing the current rate, as the peaks in DVA do.

The trend of the mechanical characteristic has an impact on possible estimation algorithms: non-monotonic mechanical deformation might complicate SOC estimation but aid SOH estimation. Conversely, SOC estimation becomes easier with a monotonic mechanical deformation, but SOH would require a greater derivative order to track the graphite stage transitions, complicating the algorithm when dealing with noisy data.

CRediT authorship contribution statement

Davide Clerici: Writing – review & editing, Writing – original draft, Visualization, Validation, Software, Resources, Methodology, Investigation, Formal analysis, Data curation, Conceptualization. **Salvatore Martelli:** Resources, Methodology, Investigation, Conceptualization. **Francesco Mocera:** Writing – review & editing, Validation, Supervision, Investigation, Conceptualization. **Aurelio Somà:** Writing – review & editing, Supervision, Resources, Project administration, Formal analysis, Conceptualization.

Declaration of competing interest

The authors declare that they have no known competing financial interests or personal relationships that could have appeared to influence the work reported in this paper.

Data availability

Data will be made available on request.

References

[1] Shedding Light on Energy - 2023 Edition, Technical Report, Eurostat, 2023, http://dx.doi.org/10.2785/405482.

[2] Sources of Greenhouse Gas Emissions, Technical Report, United state environmental protection agency, 2023.

[3] Distribution of Greenhouse Gas Emissions Worldwide in 2020, by Sector, Technical Report, Statista, 2023.

[4] S. Martelli, F. Mocera, A. Somà, Carbon footprint of an orchard tractor through a life-cycle assessment approach, Agriculture 13 (6) (2023) 1210.

[5] S. Martelli, F. Mocera, A. Somà, New Challenges Towards Electrification Sustainability: Environmental Impact Assessment Comparison Between ICE and Hybrid-Electric Orchard Tractor, 2023.

[6] Y. Zhao, P. Stein, Y. Bai, M. Al-Siraj, Y. Yang, B.X. Xu, A review on modeling of electro-chemo-mechanics in lithium-ion batteries, J. Power Sources 413 (December 2018) (2019) 259–283, http://dx.doi.org/10.1016/j.jpowsour.2018.12.011.

[7] D. Clerici, F. Mocera, A. Somà, Analytical solution for coupled diffusion induced stress model for lithium-ion battery, Energies 13 (7) (2020) 1717.

[8] D. Clerici, F. Mocera, A. Somà, Shape influence of active material micro-structure on diffusion and contact stress in lithium-ion batteries, Energies 14 (1) (2020) 134.

[9] D. Clerici, F. Mocera, Micro-scale modeling of lithium-ion battery, in: IOP Conference Series: Materials Science and Engineering, vol. 1038, (1) IOP Publishing, 2021, 012007.

[10] F. Mocera, A. Somà, D. Clerici, Study of aging mechanisms in lithium-ion batteries for working vehicle applications, in: 2020 Fifteenth International Conference on Ecological Vehicles and Renewable Energies, EVER, IEEE, 2020, pp. 1–8.

[11] D. Clerici, F. Pistorio, F. Mocera, A. Somà, Mechanical characterization and modelling of lithium-ion batteries, Transp. Res. Procedia 70 (2023) 276–283.

[12] F. Pistorio, D. Clerici, F. Mocera, A. Somà, Review on the experimental characterization of fracture in active material for lithium-ion batteries, Energies 15 (23) (2022) 9168.

[13] F. Pistorio, D. Clerici, F. Mocera, A. Somà, Coupled electrochemical-mechanical model for fracture analysis in active materials of lithium ion batteries, J. Power Sources 580 (2023) 233378.

[14] F. Pistorio, D. Clerici, F. Mocera, A. Somà, Review on the numerical modeling of fracture in active materials for lithium ion batteries, J. Power Sources 566 (2023) 232875.

[15] D. Clerici, F. Mocera, F. Pistorio, Analysis of fracture behaviour in active materials for lithium ion batteries, in: IOP Conference Series: Materials Science and Engineering, vol. 1214, (1) IOP Publishing, 2022, 012018.

[16] F. Pistorio, D. Clerici, A. Somà, Analytical computation of stress intensity factor for active material particles of lithium ion batteries, Eng. Fract. Mech. 292 (2023) 109597.

[17] H. Popp, M. Koller, M. Jahn, A. Bergmann, Mechanical methods for state determination of Lithium-Ion secondary batteries: A review, J. Energy Storage 32 (September) (2020) 101859, http://dx.doi.org/10.1016/j.est.2020.101859.

[18] B. Rieger, S.F. Schuster, S.V. Erhard, P.J. Osswald, A. Rheinfeld, C. Willmann, A. Jossen, Multi-directional laser scanning as innovative method to detect local cell damage during fast charging of lithium-ion cells, J. Energy Storage 8 (2016) 1–5.

[19] D. Clerici, F. Mocera, A. Soma, Electrochemical–mechanical multi-scale model and validation with thickness change measurements in prismatic lithium-ion batteries, J. Power Sources 542 (2022) 231735.

[20] D. Clerici, F. Mocera, A. Somà, Experimental characterization of lithium-ion cell strain using laser sensors, Energies 14 (19) (2021) 6281.

[21] R. Hickey, T.M. Jahns, Measuring individual battery dimensional changes for state-of-charge estimation using strain gauge sensors, in: 2019 IEEE Energy Conversion Congress and Exposition, ECCE, IEEE, 2019, pp. 2460–2465.

[22] L.K. Willenberg, P. Dechent, G. Fuchs, D.U. Sauer, E. Figgemeier, High-precision monitoring of volume change of commercial lithium-ion batteries by using strain gauges, Sustainability 12 (2) (2020) 557.

[23] J. Schmitt, B. Kraft, J.P. Schmidt, B. Meir, K. Elian, D. Ensling, G. Keser, A. Jossen, Measurement of gas pressure inside large-format prismatic lithium-ion cells during operation and cycle aging, J. Power Sources 478 (2020) 228661.

[24] H. Pegel, O. von Kessel, P. Heugel, T. Deich, J. Tübke, K.P. Birke, D.U. Sauer, Volume and thickness change of NMC811| SiOx-graphite large-format lithium-ion cells: from pouch cell to active material level, J. Power Sources 537 (2022) 231443.

[25] M.A.P. Estevez, F.V. Conte, C. Tremonti, M. Renzi, Aging estimation of lithium ion cells under real-world conditions through mechanical stress measurements, J. Energy Storage 64 (2023) 107186.

[26] J. Cannarella, C.B. Arnold, State of health and charge measurements in lithium-ion batteries using mechanical stress, J. Power Sources 269 (2014) 7–14.

[27] T.R. Garrick, M.A. Fernandez, M. Verbrugge, C. Labaza, R. Mollah, B.J. Koch, M. Jones, J. Gao, X. Gao, N. Irish, Quantifying volume change in porous electrodes via the multi-species, multi-reaction model, J. Electrochem. Soc. (2023).

[28] S. Hahn, S. Theil, J. Kroggel, K.P. Birke, Pressure prediction modeling and validation for lithium-ion pouch cells in buffered module assemblies, J. Energy Storage 40 (2021) 102517.

[29] O. von Kessel, T. Hoehl, P. Heugel, F. Brauchle, D. Vrankovic, K.P. Birke, Electrochemical-mechanical parameterization and modeling of expansion, pressure, and porosity evolution in NMC811| SiOx-graphite lithium-ion cells, J. Electrochem. Soc. (2023).

[30] A. Louli, L. Ellis, J. Dahn, Operando pressure measurements reveal solid electrolyte interphase growth to rank Li-ion cell performance, Joule 3 (3) (2019) 745–761.
[31] P. Mohtat, S. Lee, J.B. Siegel, A.G. Stefanopoulou, Comparison of expansion and voltage differential indicators for battery capacity fade, J. Power Sources 518 (2022) 230714.
[32] P. Mohtat, S. Lee, V. Sulzer, J.B. Siegel, A.G. Stefanopoulou, Differential expansion and voltage model for Li-ion batteries at practical charging rates, J. Electrochem. Soc. 167 (11) (2020) 110561.
[33] P. Mohtat, S. Lee, J.B. Siegel, A.G. Stefanopoulou, Towards better estimability of electrode-specific state of health: Decoding the cell expansion, J. Power Sources 427 (2019) 101–111.
[34] P. Mohtat, S. Lee, J.B. Siegel, A.G. Stefanopoulou, Reversible and irreversible expansion of lithium-ion batteries under a wide range of stress factors, J. Electrochem. Soc. 168 (10) (2021) 100520.
[35] D. Schmider, W.G. Bessler, Thermo-electro-mechanical modeling and experimental validation of thickness change of a lithium-ion pouch cell with blend positive electrode, Batteries 9 (7) (2023) 354.
[36] K.Y. Oh, J.B. Siegel, L. Secondo, S.U. Kim, N.A. Samad, J. Qin, D. Anderson, K. Garikipati, A. Knobloch, B.I. Epureanu, et al., Rate dependence of swelling in lithium-ion cells, J. Power Sources 267 (2014) 197–202.
[37] F. Grimsmann, F. Brauchle, T. Gerbert, A. Gruhle, M. Knipper, J. Parisi, Hysteresis and current dependence of the thickness change of lithium-ion cells with graphite anode, J. Energy Storage 12 (2017) 132–137.
[38] S. Mohan, Y. Kim, J.B. Siegel, N.A. Samad, A.G. Stefanopoulou, A phenomenological model of bulk force in a li-ion battery pack and its application to state of charge estimation, J. Electrochem. Soc. 161 (14) (2014) A2222.
[39] N.A. Samad, Y. Kim, J.B. Siegel, A.G. Stefanopoulou, Battery capacity fading estimation using a force-based incremental capacity analysis, J. Electrochem. Soc. 163 (8) (2016) A1584.
[40] M.A. Figueroa-Santos, J.B. Siegel, A.G. Stefanopoulou, Leveraging cell expansion sensing in state of charge estimation: Practical considerations, Energies 13 (10) (2020) 2653.
[41] S. Mohan, Y. Kim, A.G. Stefanopoulou, On improving battery state of charge estimation using bulk force measurements, in: Dynamic Systems and Control Conference, vol. 57243, American Society of Mechanical Engineers, 2015, V001T13A010.
[42] H. Dai, C. Yu, X. Wei, Z. Sun, State of charge estimation for lithium-ion pouch batteries based on stress measurement, Energy 129 (2017) 16–27.
[43] Y.J. Ee, K.S. Tey, K.S. Lim, P. Shrivastava, S. Adnan, H. Ahmad, Lithium-ion battery state of charge (SoC) estimation with non-electrical parameter using uniform fiber Bragg grating (FBG), J. Energy Storage 40 (2021) 102704.
[44] Y. Li, K. Li, X. Liu, X. Li, L. Zhang, B. Rente, T. Sun, K.T. Grattan, A hybrid machine learning framework for joint SOC and SOH estimation of lithium-ion batteries assisted with fiber sensor measurements, Appl. Energy 325 (2022) 119787.
[45] J. Peng, S. Jia, S. Yang, X. Kang, H. Yu, Y. Yang, State estimation of lithium-ion batteries based on strain parameter monitored by fiber Bragg grating sensors, J. Energy Storage 52 (2022) 104950.
[46] B. Rente, M. Fabian, M. Vidakovic, X. Liu, X. Li, K. Li, T. Sun, K.T. Grattan, Lithium-ion battery state-of-charge estimator based on FBG-based strain sensor and employing machine learning, IEEE Sens. J. 21 (2) (2020) 1453–1460.
[47] A. Knobloch, C. Kapusta, J. Karp, Y. Plotnikov, J.B. Siegel, A.G. Stefanopoulou, Fabrication of multimeasurand sensor for monitoring of a li-ion battery, J. Electron. Packag. 140 (3) (2018) 031002.
[48] S. Pannala, A. Weng, I. Fischer, J.B. Siegel, A.G. Stefanopoulou, Low-cost inductive sensor and fixture kit for measuring battery cell thickness under constant pressure, IFAC-PapersOnLine 55 (37) (2022) 712–717.
[49] Y. Plotnikov, J. Karp, A. Knobloch, C. Kapusta, D. Lin, Eddy current sensor for in-situ monitoring of swelling of Li-ion prismatic cells, in: AIP Conference Proceedings, vol. 1650, (1) American Institute of Physics, 2015, pp. 434–442.
[50] B. Rieger, S. Schlueter, S.V. Erhard, A. Jossen, Strain propagation in lithium-ion batteries from the crystal structure to the electrode level, J. Electrochem. Soc. 163 (8) (2016) A1595.
[51] D. Sauerteig, N. Hanselmann, A. Arzberger, H. Reinshagen, S. Ivanov, A. Bund, Electrochemical-mechanical coupled modeling and parameterization of swelling and ionic transport in lithium-ion batteries, J. Power Sources 378 (2018) 235–247.
[52] L. Wu, Z. Lyu, Z. Huang, C. Zhang, C. Wei, Physics-based battery SOC estimation methods: Recent advances and future perspectives, J. Energy Chem. (2023).
[53] E. Vergori, F. Mocera, A. Somà, Battery modelling and simulation using a programmable testing equipment, Computers 7 (2) (2018) 20.
[54] Z. Cui, L. Wang, Q. Li, K. Wang, A comprehensive review on the state of charge estimation for lithium-ion battery based on neural network, Int. J. Energy Res. 46 (5) (2022) 5423–5440.
[55] B. Jiang, S. Tao, X. Wang, J. Zhu, X. Wei, H. Dai, Mechanics-based state of charge estimation for lithium-ion pouch battery using deep learning technique, Energy 278 (2023) 127890.
[56] R. Li, D. Ren, D. Guo, C. Xu, X. Fan, Z. Hou, L. Lu, X. Feng, X. Han, M. Ouyang, Volume deformation of large-format lithium ion batteries under different degradation paths, J. Electrochem. Soc. 166 (16) (2019) A4106.
[57] A.G. Stefanopoulou, N.A. Samad, Y. Kim, J.B. Siegel, State of battery health estimation based on swelling characteristics, 2016.
[58] A. Fortier, Embedded sensors for in-situ cell monitoring of batteries, 2017.
[59] J.Q. Xu, J. Steiber, C.M. Wall, R. Smith, N. Cheuk, Strain measurement based battery testing, 2013.
[60] E. Poirier, T.Q. Tran, B.A. Tabatowski-Bush, Sensitive strain-based soc and soh monitoring of battery cells, 2017.
[61] C.B. Arnold, J. Cannarella, Device and method for mechanically detecting anomalous battery operation, 2017.
[62] C.B. Arnold, J. Cannarella, Mechanical measurement of state of health and state of charge for intercalation batteries, 2013.
[63] A. Somà, F. Mocera, Device and method to measure and estimation of state of charge and state of health of a battery, 2022.
[64] B. Rieger, S.V. Erhard, K. Rumpf, A. Jossen, A new method to model the thickness change of a commercial pouch cell during discharge, J. Electrochem. Soc. 163 (8) (2016) A1566.
[65] K.E. Thomas, J. Newman, Heats of mixing and of entropy in porous insertion electrodes, J. Power Sour. 119 (2003) 844–849.
[66] A.K. Padhi, K.S. Nanjundaswamy, J.B. Goodenough, Phospho-olivines as positive-electrode materials for rechargeable lithium batteries, J. Electrochem. Soc. 144 (4) (1997) 1188.
[67] R. Koerver, W. Zhang, L. de Biasi, S. Schweidler, A.O. Kondrakov, S. Kolling, T. Brezesinski, P. Hartmann, W.G. Zeier, J. Janek, Chemo-mechanical expansion of lithium electrode materials–on the route to mechanically optimized all-solid-state batteries, Energy Environ. Sci. 11 (8) (2018) 2142–2158.
[68] C. Didier, W.K. Pang, Z. Guo, S. Schmid, V.K. Peterson, Phase evolution and intermittent disorder in electrochemically lithiated graphite determined using in operando neutron diffraction, Chem. Mater. 32 (6) (2020) 2518–2531, http://dx.doi.org/10.1021/acs.chemmater.9b05145.
[69] N. Iqbal, J. Choi, C. Lee, H.M.U. Ayub, J. Kim, M. Kim, Y. Kim, D. Moon, S. Lee, Effects of diffusion-induced nonlinear local volume change on the structural stability of NMC cathode materials of lithium-ion batteries, Mathematics 10 (24) (2022) 4697.
[70] M. Lewerenz, A. Marongiu, A. Warnecke, D.U. Sauer, Differential voltage analysis as a tool for analyzing inhomogeneous aging: A case study for LiFePO4| Graphite cylindrical cells, J. Power Sources 368 (2017) 57–67.